Non-contacting measurements of photocarrier lifetimes in bulk- and polycrystalline thin-film Si photoconductive devices by photothermal radiometry

A. Mandelis,[a),b)] A. Othonos, and C. Christofides
Department of Natural Sciences, Faculty of Pure and Applied Sciences, University of Cyprus, P.O. Box 537, Nicosia, Cyprus

J. Boussey-Said
Laboratoire de Physique des Composants a Semiconducteur, URA CNRS 840, 23 rue des Martyrs, B.P. 257, 38031 Grenoble Cedex 1, France

(Received 11 July 1996; accepted for publication 5 August 1996)

Laser-induced and frequency-scanned infrared photothermal radiometry was applied to a crystalline-Si photoconductive device, and to polysilicon thin-film photoconductors deposited on oxidized Si substrates by an LPCVD method. A detailed theoretical model for the radiometric signal was developed and used to measure the free photoexcited carrier plasma recombination lifetime, electronic diffusivity and surface recombination velocity of these devices, with the simultaneous measurement of the bulk thermal diffusivity. A trade-off between detectivity/gain and frequency-response bandwidth was found via the lifetime dependence on the wafer background temperature rise induced by Joule-heating due to the applied bias. This effect was most serious with the bulk-Si device, but was limited by the high resistivity of the LPCVD thin-film devices. In the case of the bulk-Si device, the results of photothermal radiometry were compared with, and corroborated by, frequency-scanned photocurrent measurements. More sophisticated analysis was shown to be required for the interpretation of the polysilicon photoconductor frequency-responses, perhaps involving the fractal nature of carrier transport in these grain-structured devices. © *1996 American Institute of Physics.* [S0021-8979(96)10121-3]

I. INTRODUCTION

Since the early photoacoustic studies of transport photoconductive phenomena in semiconductors,[1–3] an increasing amount of work has been reported in exploiting thermal- and carrier diffusion-wave effects in substrate Si wafers[4] and in active photoexcited devices[5] by means of infrared photothermal radiometry. The utility of this technique lies in its ability to yield electronic transport measurements in a nondestructive, noncontacting manner and, more fundamentally, in exploring near-surface electronic processes in semiconductors without the requirement for electrical contacts which are known to perturb the energetics of the interface.[6] Very recently we were able to identify a surface acceptor state in undoped semi-insulating GaAs by photothermal radiometric deep-level transient spectroscopy,[7] which had previously remained hidden under the pinning of the Fermi level at the metal-semiconductor interface by the presence of the metallic contact. The advantage of photothermal radiometry over other photothermal techniques applied to semiconductor characterization[8] is the domination of the signal by the carrier plasma-wave component in high-quality samples,[5] especially at laser-beam modulation frequencies above the inverse of the thermal transit time in the material. Nevertheless, care must be taken in interpreting data, as it has been shown[9] that, with some bulk semiconductors with a history of surface processing, the thermal-wave-induced blackbody component may dominate the radiometric signal, which then becomes insensitive to electronic transport phenomena.

In this work radiometric signals from electroded photoconductor devices, both bulk and thin-film, have been investigated and the full theoretical framework for the analysis of such signals has been developed, including photocurrent (PC) frequency scans. It was found that, under considerations of the full (plasma- and thermal-wave) infrared photothermal radiometric (PTR) response, carrier plasma transport processes can be monitored in both high-quality substrates and in deposited and processed thin films. It will be shown that PTR can yield measurements of the especially important, device-gain-determining recombination lifetime and can further reveal its dependence on the dc temperature of the photoconductive device, owing to Joule-heating under the applied bias.

II. MATERIALS AND EXPERIMENT

Substrate n-type Si wafers, of resistivity $\rho=20\ \Omega\,\mathrm{cm}$, were oxidized thermally at 1150 °C for 17 h. The oxidation was followed by low-pressure chemical vapor deposition (LPCVD) at 630 °C and 500 mTorr of thin polycrystalline Si films 1 μm thick. The thin films were implanted with P^+ ions at 200 keV and fluences of up to $10^{15}\ \mathrm{cm}^{-2}$, followed by a thermal anneal at 1000 °C for 1 h, in order to electrically activate the implanted impurities and stabilize the grain size. Inspection with electron microscopy revealed a grain size of $\approx$500 Å. Subsequently, conducting electrodes were formed

[a)]On leave from the Photothermal and Optoelectronic Diagnostics Laboratory, Department of Mechanical and Industrial Engineering, University of Toronto, Toronto M5S 3G8, Canada.
[b)]Electronic mail: mandelis@me.utoronto.ca

 0021-8979/96/80(9)/5332/10/$10.00

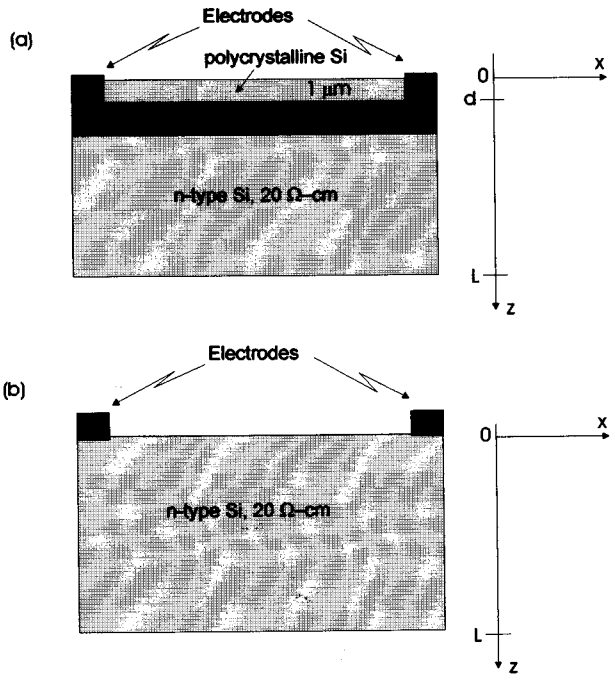

FIG. 1. Cross-sectional views of the photoconductive Si devices: (a) Thin-film photoconductor; (b) Substrate-Si photoconductor. For fabrication parameters see text.

using an LPCVD-deposited masking oxide 0.7 μm thick and a photolithographic mask, followed by doping of the contact oxide regions by P^+-ion implantation at 120 keV and 10^{16} cm^{-2}, activated at 950 °C for 1 h in a neutral ambient. The contacts were further metallized by aluminum evaporation using another mask level, followed by thermal diffusion at low temperature (450 °C, 30 min). Finally, the remaining masking oxide was lifted and several dice were cut and placed on ceramic chips. The cross-section of the resulting photoconducting devices is shown in Fig. 1(a). In this investigation attention was focused on the highest doping-density photoconductors (1×10^{15} cm^{-2}), as they exhibited the strongest free-carrier plasma responses.

In addition, and for comparison purposes, bulk photoconducting devices were also fabricated on substrate Si wafers. This process involved only the deposition of the masking oxide and the formation of conductive contacts on the otherwise unprocessed substrate [Fig. 1(b)].

The photoconductive devices were investigated by PTR using the experimental setup of Fig. 2. The photoexcitation source was a CW Ar-Kr mixed gas laser from Coherent (Innova 70) emitting at mixed 488 and 514.5 nm. The gently focused beam size was ≈1 mm, with output power on the order of 100 mW. The intensity of the laser was acousto-optically modulated using an external sine-wave generator to automatically change the modulation frequency. The blackbody radiation emitted from the semiconductor was collected by means of two collimating, off-axis, Ag-coated, paraboloidal mirrors and was focused onto a wide-bandwidth, liquid-nitrogen-cooled, photoconductive HgCdTe (MCT) detector with spectral response range between 2 and 12 μm. The MCT detector/preamplifier circuit had a combined frequency

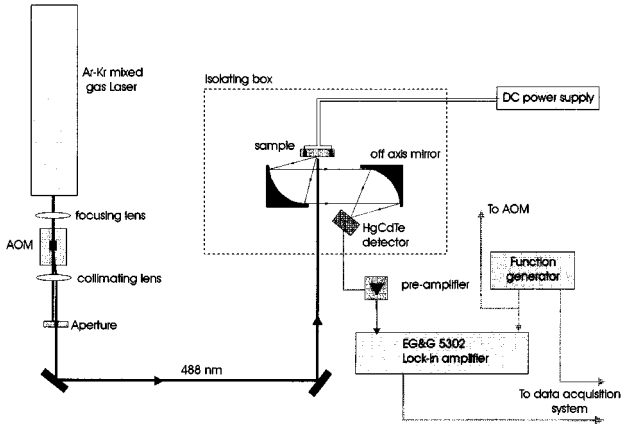

FIG. 2. Experimental setup of infrared photothermal radiometry of bulk and thin-film Si photoconductors.

bandwidth between 1 Hz and 1 MHz. The detector was fitted with a Ge window, which filtered out the excitation beam. The PTR signal from the preamplifier (EG and G Judson Model PA-350) was fed into a lock-in analyzer (EG and G Model 5302). Normalized amplitude and phase curves were obtained automatically, as it was verified that the data from a reference Si wafer in the 1 Hz–1 MHz range could be accurately fitted to a simple theoretical model of a single excited-state relaxation lifetime,[9] without any further corrections.

The PC signal of some wafers was also monitored with the setup shown in Fig. 3, which is a modification of the setup of Fig. 2. The ac voltage-drop across a small resistor of known resistance value carrying the photocurrent was fed into the lock-in amplifier and the amplitude and phase were recorded as functions of the laser-beam-intensity modulation frequency with the dc electric field applied across the electrodes of the photoconductor as a parameter. The ac voltage drop is proportional to the photocurrent generated by the optical excitation of the sample. In opposition to direct photocurrent measurements in series, the parallel-circuit geometry of Fig. 3 has the advantage of presenting high-

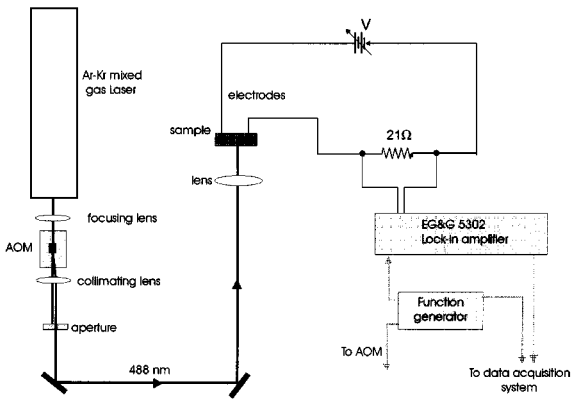

FIG. 3. Experimental setup of photocurrent frequency-response measurements of bulk and thin-film Si photoconductors.

impedance probes to the terminals of the known resistor, thus consuming no current during the measurement.

III. THEORETICAL

A. Principles of semiconductor PTR

In the geometry of Fig. 1, the lateral dimensions ($\sim$4 mm) of the photoconductive device are assumed to be infinite compared to the spot size of the laser beam, so that any edge effects may be ignored. Furthermore, the 1-mm spot-size laser beam was large enough to assure the one-dimensionality of the PTR and PC signals, as its lateral dimension was large compared to the thermal- and electron-diffusion length in Si.[10]

For harmonically modulated optical excitation with superbandgap radiation, the IR absorption coefficient, α_{IR}, is a function of the free-carrier density in the semiconductor:[11]

$$\alpha_{\mathrm{IR}}(z;\omega,\lambda)=\alpha^{o}_{\mathrm{IR}}(z,\lambda)+\Delta\alpha(z,\lambda)e^{i\omega t}, \tag{1}$$

where the right-hand-side terms stand for the IR absorption coefficient in the dark (no illumination) and due to photoexcited free carriers at modulation frequency $f=\omega/2\pi$, respectively. The temperature rise in the semiconductor due to lattice absorption, intraband de-excitation, and hot-electron interband recombination is

$$\Theta(z,t)=\Theta_o+\Delta\Theta(z)e^{i\omega t}. \tag{2}$$

After a Taylor expansion around the ambient value of the temperature, and retention of the first-order term only, the change in Planck's distribution function is, accordingly,

$$W_P[\Theta(z,t),\lambda]\approx W_P(\Theta_o,\lambda)+\Delta W_P(z,\lambda,\omega)e^{i\omega t}, \tag{3}$$

where

$$W_P(\Theta,\lambda)=\frac{2\pi hc^2A}{\lambda^5[\exp(hc/\lambda k_B\Theta)-1]} \tag{4}$$

and

$$\Delta W_P(z,\lambda,\Theta_o)=W_P(\lambda,\Theta_o)\,\frac{hc/\lambda k_B\Theta_o}{\exp(hc/\lambda k_B\Theta_o)-1}\times\frac{\Delta\Theta(z,\omega)}{\Theta_o}. \tag{5}$$

In Eqs. (4) and (5) k_B, h, and c have their usual meanings; A is the emitting surface area, and λ is the emission (infrared) wavelength. According to a statement of Kirchhoff's law reflecting conservation of energy, ''at thermodynamic equilibrium the rate of emission of blackbody radiation from the surface and throughout the bulk of a material is exactly equal to the rate of absorption of radiation incident on the material per wavelength interval.'' Although the above statement is strictly valid under equilibrium conditions, in practice it has been found to be of broader validity[12] and applicability to several nonequilibrium processes in semiconductors.[13] Therefore, the infrared emission spectrum for a de-excitation process in a semiconductor can be obtained directly from its (usually better-known) absorption spectrum. Mandelis *et al.* have given a detailed discussion of the applicability of Kirchhoff's law to the generation of dynamic PTR signals.[14]

The total radiation power per wavelength (W/μm) at the front surface arriving from the interior of a wafer of thickness L, with the back surface unpolished so as to neglect multiple reflections is[5]

$$P(\omega,\lambda)=\int_0^L\alpha_{\mathrm{IR}}(z;\omega,\lambda)\exp\left[-\int_0^z\alpha_{\mathrm{IR}}(y;\omega,\lambda)dy\right]\times W_P[\Theta(z,t)]dz. \tag{6}$$

Assuming that $L\leqslant 500$ μm and any process-related surface damage layer is no deeper than 1 μm, and furthermore taking into account that the photoinjected carrier density is limited to $\approx 10^{19}$ cm^{-3} by lifetime reduction due to Auger recombinations, the expression for $P(\omega,\lambda)$ results in contributions to the dc, ω, and 2ω radiation fields. Consistently with the filtering action of the lock-in amplifier, selection of the linear ($\propto\omega$) terms only gives

$$P(\omega,\lambda)=\int_0^L\alpha^{o}_{\mathrm{IR}}(z,\lambda)\Delta W_P(z;\omega,\lambda)dz+\int_0^L W_P(\Theta_o,\lambda)\Delta\alpha(z;\omega,\lambda)dz \tag{7}$$

where the $\exp(i\omega t)$ terms were suppressed (demodulation). Finally, an expression for the linear PTR signal can be found assuming a depth-independent $\alpha^{o}_{\mathrm{IR}}(\lambda)$ and considering a classical model for wave propagation in a free plasma:[15]

$$S_{\mathrm{PTR}}(\omega,\alpha_{\mathrm{vis}})=a(\lambda_{\mathrm{vis}},\Theta_o,\lambda_1,\lambda_2)\int_0^L\Delta\Theta(z;\alpha_{\mathrm{vis}},\omega)dz+b(\lambda_{\mathrm{vis}},\Theta_o,\lambda_1,\lambda_2)\int_0^L\Delta N(z;\alpha_{\mathrm{vis}},\omega)dz. \tag{8a}$$

The coefficients a and b are independent of the modulation frequency, but they depend on temperature and on the spectral range of the MCT detector (λ_1,λ_2). They are given by the following expressions:

$$a=[1-R(\lambda_{\mathrm{vis}})]\int_{\lambda_1}^{\lambda_2}[1-R(\lambda)]W_P(\lambda,\Theta_o)\times\frac{hc\alpha^{o}_{\mathrm{IR}}(\lambda)d\lambda}{\lambda k_B\Theta_o^2[\exp(hc/\lambda k_B\Theta_o)-1]} \tag{8b}$$

and

$$b=[1-R(\lambda_{\mathrm{vis}})]\int_{\lambda_1}^{\lambda_2}[1-R(\lambda)]W_P(\lambda,\Theta_o)\times\frac{\lambda^2q^3d\lambda}{4\pi^2c^3n\epsilon_o m^{*2}\mu_n}, \tag{8c}$$

where q is the elementary charge, m^* is the effective mass of the photoexcited carriers and μ_n is their mobility, ϵ_o is the dielectric constant of vacuum. Here it is assumed that electronic transport occurs via *excess* n-type carriers, consistently with the types of samples employed in the experiments. For harmonically modulated incident laser intensity,

absorbed in the body of the semiconductor according to Beer's law, which excites the excess photocarriers,

$$I(z,\omega)=\frac{\alpha\eta_Q I_o e^{-\alpha z}}{2h\nu}(1+e^{i\omega t}), \tag{9}$$

where $\alpha=\alpha_{\rm vis}$, and I_o is the intensity of the incident radiation of optical frequency ν; η_Q is the quantum efficiency of the carrier generation process and will be taken to be unity.

For 1D diffusive propagation of the photocarriers along the depth (z) direction of a semiconductor of thickness L (Fig. 1), the equation for the excess free-carrier density, $\Delta N(z,\omega)$, has been presented by Sheard and Somekh,[9] but is given in a corrected form here:

$$\Delta N(z,\omega)=\frac{\alpha\eta I_o}{h\nu D(\alpha^2-\sigma_e^2)}\left[\left[G_1G_2\left[\frac{g_1-g_2e^{-(\alpha+\sigma_e)L}}{G_2-G_1e^{-2\sigma_eL}}\right]\right.\right.$$
$$\times e^{-\sigma_e z}-e^{-\alpha z}\left[\frac{g_1G_1-g_2G_2e^{-(\alpha-\sigma_e)L}}{G_2-G_1e^{-2\sigma_eL}}\right]$$
$$\left.\left.\times e^{-\sigma_e(2L-z)}\right]\right], \tag{10}$$

where the following definitions were made:

$$G_1\equiv\frac{D\sigma_e-s_1}{D\sigma_e+s_1},\quad G_2\equiv\frac{D\sigma_e+s_2}{D\sigma_e-s_2};$$
$$g_1\equiv\frac{D\alpha+s_1}{D\sigma_e-s_1},\quad g_2\equiv\frac{D\alpha-s_2}{D\sigma_e+s_2}. \tag{11}$$

Here, s_j and $j=1,2$ are surface recombination velocities at the upper (1) and back (2) surfaces of the semiconductor, D is the carrier diffusion coefficient, and σ_e is the plasma-wave complex wave number, the inverse of the carrier complex diffusion length, defined as

$$\sigma_e(\omega)\equiv\sqrt{\frac{1+i\omega\tau}{D\tau}}, \tag{12}$$

with τ being the recombination lifetime of the semiconductor.

Equation (10), when integrated over the thickness of the (essentially infrared-transparent, but opaque in the visible region: $\alpha L\gg 1$) Si wafer, as per the requirement of the total PTR signal expression [Eq. (8a)], yields the result

$$\int_0^L\Delta N(z,\omega)dz=\frac{I_o(1-e^{-\sigma_eL})}{h\nu(D\sigma_e+s_1)\sigma_e}\left[\frac{G_2+e^{-\sigma_eL}}{G_2-G_1e^{-2\sigma_eL}}\right]. \tag{13}$$

B. The thermal-wave field in bulk photoconductor Si devices

In the presence of an applied bias, the thermal-wave field in the semiconductor of Fig. 1(b) is given by

$$\frac{d^2}{dz^2}\Delta\Theta(z,\omega)-\sigma_t\Delta\Theta(z,\omega)=-\frac{H(z,\omega)}{k}, \tag{14a}$$

where the thermal source term H contains components due to nonradiative intraband de-excitation, nonradiative interband carrier recombination, and Joule-effect heating:[16]

$$H(z,\omega)=\frac{\eta(h\nu-E_g)}{h\nu}\alpha I_o e^{-\alpha z}+\frac{E_g}{\tau}\Delta N(z,\omega)$$
$$+\mathbf{E}\cdot\mathbf{J}(z,\omega). \tag{14b}$$

Here η is the optical-to-thermal energy conversion efficiency, taken to be equal to 1 in Si, σ_t is the complex thermal diffusion coefficient,

$$\sigma_t=\sqrt{i\omega/\beta}, \tag{14c}$$

β is the thermal diffusivity of the semiconductor, k is the thermal conductivity, $\mathbf{E}$ is the applied transverse electric field between the electrodes (x-direction in Fig. 1), $\mathbf{J}$ is the transverse current density, and E_g is the energy gap.

The differential equation for the thermal-wave field is subject to boundary conditions involving the surface recombination velocities:

$$-k\frac{d}{dz}\Delta\Theta(z,\omega)\bigg|_{z=0}=s_1\Delta N(0,\omega)E_g \tag{15a}$$

and

$$k\frac{d}{dz}\Delta\Theta(z,\omega)\bigg|_{z=L}=s_2\Delta N(L,\omega)E_g. \tag{15b}$$

To determine the term $\mathbf{E}\cdot\mathbf{J}$, use will be made of the experimental fact that the photocurrent data from the bulk samples were consistent with a contribution from only the drift component. Therefore, the diffusion current density along the x-direction (Fig. 1) was neglected

$$\mathbf{E}\cdot\mathbf{J}(z,\omega)=q\mu E^2\Delta N(z,\omega). \tag{16}$$

The solution to the boundary-value problem of Eqs. (14)–(16) involves considerable algebra. For the thermal-wave component of the PTR signal generation in the geometry of Fig. 1(b), however, only the optically opaque limit is needed in the form $\int_0^L\Delta\Theta(z,\omega)dz$, according to Eq. (8a). The result is

$$\int_0^L\Delta\Theta(z,\omega)dz=\frac{1}{\sigma_t}[(1-e^{-\sigma_tL})F_1+F_2]-\frac{C_0N_o}{\sigma_e}$$
$$\times(1-e^{-\sigma_eL})(G_2+e^{-\sigma_eL}), \tag{17}$$

where the following definitions have been made:

$$F_1\equiv\frac{C_1+C_2e^{-\sigma_tL}}{1-e^{-2\sigma_tL}}, \tag{18a}$$

$$F_2\equiv\frac{C_1e^{-\sigma_tL}+C_2}{1+e^{-\sigma_tL}}, \tag{18b}$$

$$N_o\equiv\frac{I_o}{h\nu(D\sigma_e+s_1)(G_2-G_1e^{-2\sigma_eL})}. \tag{18c}$$

Furthermore, the coefficients C_j and $j=0,1,2$ are defined

$$C_0\equiv\frac{E_g+q\mu_n\tau E^2}{k\tau(\sigma_e^2-\sigma_t^2)} \tag{19}$$

and

$$C_1 \equiv \frac{I_o(h\nu - E_g)}{h\nu k\sigma_t} + \frac{N_o}{\sigma_t k}\left[\left[s_1 E_g(G_2 + e^{-2\sigma_e L}) + \sigma_e k C_0(G_2 - e^{-2\sigma_e L})\right]\right] \tag{20a}$$

$$C_2 \equiv \frac{N_o e^{-\sigma_e L}}{\sigma_t}\left[\frac{s_2 E_g(G_2+1)}{k} + \sigma_e C_0(1-G_2)\right]. \tag{20b}$$

C. The plasma-wave field in thin-film photoconductor Si devices

In the geometry of Fig. 1(a) the grown oxide acts as an electrical insulator between the surface polysilicon thin film and the substrate. The combined thickness of the poly-Si and SiO_2 buffer layers is much smaller than the thermal diffusion length $\mu(\omega) = |\sigma_t(\omega)|^{-1}$ and the electronic carrier diffusion length $\mu_e(\omega) = |\sigma_e(\omega)|^{-1}$ in the given structure, even at the highest attainable modulation frequency of 1 MHz. Therefore, the only expected contribution to the PTR signal from the two thin layers is one of a surface source due to the plasma-wave in the poly-Si plus any thermal-wave contribution due to nonradiative relaxation in this layer. The transparent, electronically inert oxide can, at most, contribute effectively as a thermal ac impedance, in series with the poly-Si and the substrate crystalline Si. This possibility was modeled as a boundary condition[17] and tested computationally. It was found that the role of any thermal impedance due to the 2.4-μm-thick oxide was negligible. The number density of free carriers in the 1-μm-thick photoconductive poly-Si film cannot be depth-resolved by the PTR apparatus of Fig. 2 even at the highest frequencies, because the film thickness $d \ll |\sigma_e(\omega_{\max})|^{-1}$. Therefore, the quantity of interest is the depth-averaged excess carrier density

$$\langle \Delta N(x,\omega)\rangle = \int_0^d \Delta N(x,z;\omega)\,dz, \tag{21}$$

which is likely to vary in the transverse direction (x), due to electronic traps and imperfections germane to the grain-type structure of the photoconductor. Assuming the existence of internal microscopic electric fields, e.g., across grain boundaries, the equation of conservation of charge in the transverse direction can be written[18,19]

$$\frac{d^2}{dx^2}\langle \Delta N(x,\omega)\rangle - (\mu_n E_x/D)\frac{d}{dx}\langle \Delta N(x,\omega)\rangle - \sigma_{ef}^2(\omega)\langle \Delta N(x,\omega)\rangle = -\frac{1}{D} f(x,\omega), \tag{22a}$$

where σ_{ef} denotes the complex plasma wave number in the thin-film region: In practice, Eq. (12) describes this quantity, with τ being replaced by τ_f and D by D_f. E_x represents the total electric field (external and internal) along the x-direction, and the usual boundary conditions at the upper and lower surfaces of the thin film apply,[17] under the assumption of equal recombination velocities $(s_{1f} = s_{2f} = s)$ due to the essential symmetry in the deposition process. These give the source term

$$f(x,\omega) = \frac{1}{d}\left[\left[\frac{I_o(1-e^{-\alpha_f d})}{h\nu} - s[\Delta N(x,0;\omega) + \Delta N(x,d;\omega)]\right]\right], \tag{22b}$$

where α_f stands for the optical absorption coefficient of the thin poly-Si film at the excitation wavelength of the laser beam. It can be seen that the terms proportional to the boundary values of the plasma-wave field in the thin film act like carrier sinks and can be calculated from the carrier diffusion equation in the z-direction [Eq. (10)]. This equation can be used to determine $N(x,0;\omega)$ and $N(x,d;\omega)$ in the expression for $f(x,\omega)$:

$$f(x,\omega) = f(\omega) = \frac{I_o}{h\nu d}\left[\left[1 - e^{-\alpha_f d} - \frac{s\alpha_f}{D(\alpha_f^2 - \sigma_{ef}^2)} \times \left(\frac{1+e^{-\sigma_{ef}d}}{G_2 - G_1 e^{-2\sigma_{ef}d}}\left[G_1 G_2(g_1 - g_2 e^{-(\alpha_f+\sigma_{ef})d}) + (g_1 G_1 - g_2 G_2 e^{-(\alpha_f-\sigma_e)d})e^{-\sigma_e d}\right] - (1+e^{-\alpha_f d})\right)\right]\right]. \tag{23}$$

In Eq. (23) the assumption was made of uniform illumination of the semiconductor surface, so that I_o and the boundary values of the excess carrier densities are not functions of the transverse coordinate. Equation (22) may now be solved conveniently using a Green's function approach to the plasma-wave problem akin to the one developed earlier for thermal waves.[20] Neglecting source/sink contributions from the cross-sectional surface areas with unit normal vectors perpendicular to the z-direction, Fig. 1, the standard Green's function treatment,[19] yields

$$\langle \Delta N(x,\omega)\rangle = \int_0^W f(x_o,\omega)G(x-x_o,\omega)\,dx_o - \mu_n E_x \times \int_0^W \left[G(x-x_o,\omega)\frac{d}{dx_o}\langle \Delta N(x_o,\omega)\rangle - \langle \Delta N(x_o,\omega)\rangle \frac{d}{dx_o}G(x-x_o,\omega)\right]dx_o, \tag{24}$$

where W is the spot size of the (uniformly) photoexcited area of the thin-film photoconductor and $G(x-x_o,\omega)$ has the form

$$G(x-x_o,\omega) = \frac{1}{\sqrt{2}DS_e(\omega)}\exp[-\Sigma_e(\omega)|x-x_o|], \tag{25a}$$

with the effective complex plasma-wave numbers

$$S_e(\omega) = \sqrt{\sigma_{ef}^2(\omega) + (\mu_n E_x/2D)^2} \tag{25b}$$

and

$$\Sigma_e(\omega) = S_e(\omega) - (\mu_n E_x/2D), \tag{25c}$$

where the electronic diffusivity was assumed to be isotropic. Equation (24) eventually gives the depth-averaged carrier plasma density

$$\langle \Delta N(W,\omega)\rangle = \frac{f(\omega)[(\mu_n E_x/D)-\Sigma_e(\omega)]}{D\Sigma_e(\omega)[\sqrt{2}S_e(\omega)+(\mu_n E_x D)]} \times[1-e^{-\Sigma_e(\omega)W}] \tag{26}$$

subject to the boundary condition $\langle N(0,\omega)\rangle=0$.

D. The thermal-wave field in thin-film photoconductor Si devices

The calculation methodology for the PTR signal from the device geometry of Fig. 1(a) requires the integral of the plasma-and thermal-wave fields over the *entire* sample thickness L, according to Eq. (8). The former can be found from the theoretical considerations of Sec. III C. Assuming negligible thickness of the thin-film layer: $d \ll L$, one obtains

$$\int_0^L \Delta N_T(z;\omega)dz = \langle \Delta N(\omega)\rangle d + \int_0^L \Delta N(z;\omega)dz, \tag{27}$$

where the terms on the right-hand side are given by Eqs. (26) and (13), respectively. The thermal-wave problem proceeds in a manner similar to the one developed in Sec. III B. In the present case, however, the new source term is

$$H_1(z,\omega) = \left(\frac{h\nu - E_g}{h\nu}\right)\alpha I_o e^{-(\alpha_f d+\alpha z)} + \frac{E_g}{\tau}\, e^{-\alpha_f d}\Delta N(z,\omega), \tag{28}$$

subject to boundary condition (15b) and to the modified boundary condition

$$-k\,\frac{d}{dz}\,\Delta\Theta_T(z,\omega)\bigg|_{z=0} = (sE_g + q\mu_n E_x^2 W)\langle \Delta N(\omega)\rangle + s_1 \Delta N(0,\omega)E_g, \tag{29}$$

which replaces Eq. (15a). It should be noted that there is no current source in the substrate Si, which is also partly photoexcited by the fraction of the incident beam that penetrates the 1-μm-thick poly-Si layer, as the insulating oxide layer prevents this from occurring. This has been verified experimentally by measuring zero photocurrent from the low-dose implanted photoconductor thin films ($\leqslant 5\times10^{14}$ cm^{-2} P$^+$) of identical fabrication and geometry to that depicted in Fig. 1(a).

The resulting expressions for the thermal-wave field are therefore similar to Eqs. (18)–(20), with the following changes:

(i) I_o must be replaced by $I_o \exp(-\alpha_f d)$ in Eqs. (18c) and (20a);

(ii) $E=0$ in Eq. (19);

(iii) Inside the heavy brackets of Eq. (20a) an additional term

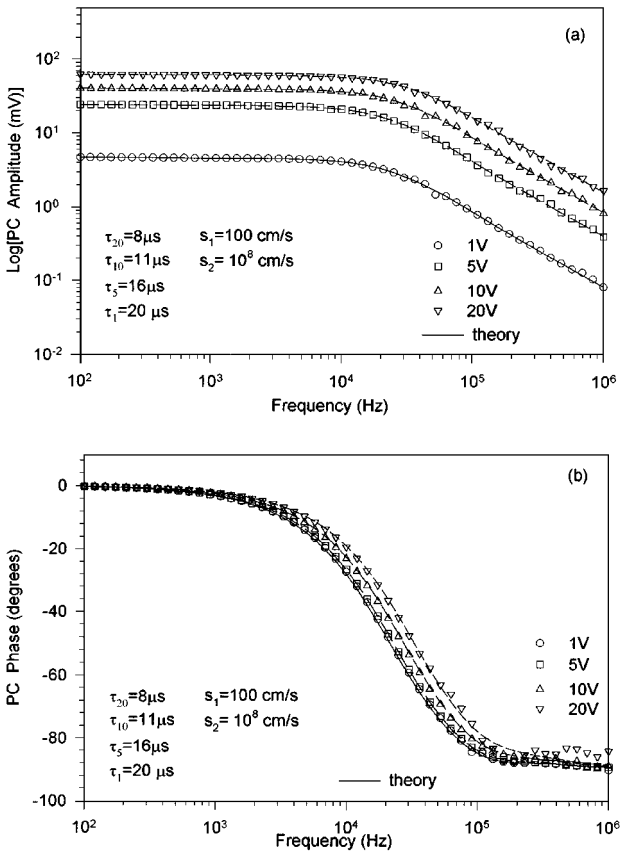

FIG. 4. Amplitude (a) and phase (b) of the photocurrent frequency scans of the substrate-Si photoconductor. Parameters of simultaneous best fits: $D=20$ cm^2/s; $L=250$ μm; $s_1=10^2$ cm/s; $s_2=10^8$ cm/s. τ_j indicates the best-fit lifetime at applied dc voltage (j).

$$(E_g s + Wq\mu_n E_x^2)\,\frac{\langle \Delta N(\omega)\rangle}{N_o}$$

must be added to the existing two terms.

IV. RESULTS AND DISCUSSION

A. Bulk Si photoconductors

The PC frequency scan of the photoconductor of geometry Fig. 1(b) is shown in Fig. 4. This type of measurement is complementary to the PTR response and is generally simpler to interpret, as it carries only electronic transport information. Of course, its main disadvantage is its contacting nature and the need for depositing ohmic contacts on the semiconductor. The theoretical interpretation of the data assumed a purely drift-current mechanism at each depth z, and a total current density J_n consisting of all the individual elementary-layer dz contributions to the collecting electrodes:

$$J_n(z,\omega) = q\mu_n E \int_0^L \Delta N(z,\omega)dz. \tag{30}$$

Furthermore, it was assumed that there was no plasma concentration gradient along the transverse (x) direction. The depth-dependence of the excess carrier density is given by Eq. (13). Equation (30) predicts a linear dependence of

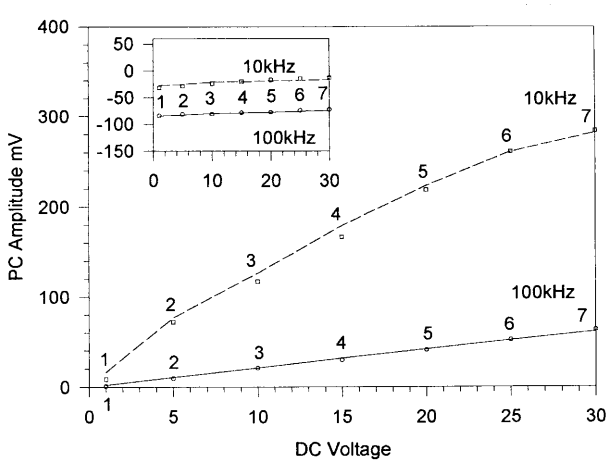

FIG. 5. Dependence of PC signal amplitude and phase (insets) on applied dc bias of the bulk Si photoconductor for $f=10$ kHz and 100 kHz. Numbered points: Theoretical best fits of Eq. (30) to the data for *both* modulation frequencies with $\mu_n=0.135$ m^2/V s (Ref. 23) and [τ (μs), D (cm^2/s)] pairs: (1: 20, 18); (2: 15, 17); (3: 10, 17); (4: 9, 17); (5: 8, 17); (6: 7, 16); and (7: 6, 16).

the PC signal on the strength of the applied electric field E. The results of the theoretical fits are shown in Fig. 4 for various applied transverse voltages. The fits of both amplitude and phase curves were excellent, provided the carrier recombination lifetime was adjusted for each voltage. It was found that the actual value of the electronic diffusivity D was not crucial to the fits, as long as it lies between 16 and 20 cm^2/s. The fits were sensitive to the value of s_1 which determined the slope of the amplitude decay, whereas the value of s_2 was relatively unimportant, as long as it was much larger than s_1, in agreement with earlier findings by Sheard *et al.* using PTR signals.[4] Physically, this is as expected, since the back surface of the wafers was not polished and therefore presented a large specific area for recombination. The PC signal fittings were most sensitive to the recombination lifetime values, which decreased with increasing applied dc voltage. This suggests that the dc temperature increase of the sample due to Joule-heating affects the lifetime values in a manner consistent with the Shockley-Reed-Hall recombination mechanism.[21] The best-fitted τ and D values are well within the accepted norms of recombination lifetimes in Si.[4,22] Figure 5 shows the PC signal (amplitude and phase) vs applied voltage $V_{\rm dc}$ data at two modulation frequencies. The electric-field E values utilized in the PC and the PTR signal fits were $E=V_{\rm dc}/2\times10^{-3}$ V/m, reflecting the lateral dimensions of the sample. Equation (30) predicts a strictly linear dependence of the signal amplitude on E, with no dependence of the signal phase. The data were best fitted to the theory, however, by adjusting the value of τ for every value of the applied voltage. The resulting values were found to be consistent for both signal channels and both modulation frequencies, Fig. 5, and exhibit considerable decreases of τ, as well as slight decreases of D, as $V_{\rm dc}$ increases. The importance of this finding rests with the potential limitations of the bulk crystalline Si photoconductor to operate under high bias to improve its gain and detectivity, which seems to bring about a narrowing of its frequency response bandwidth.

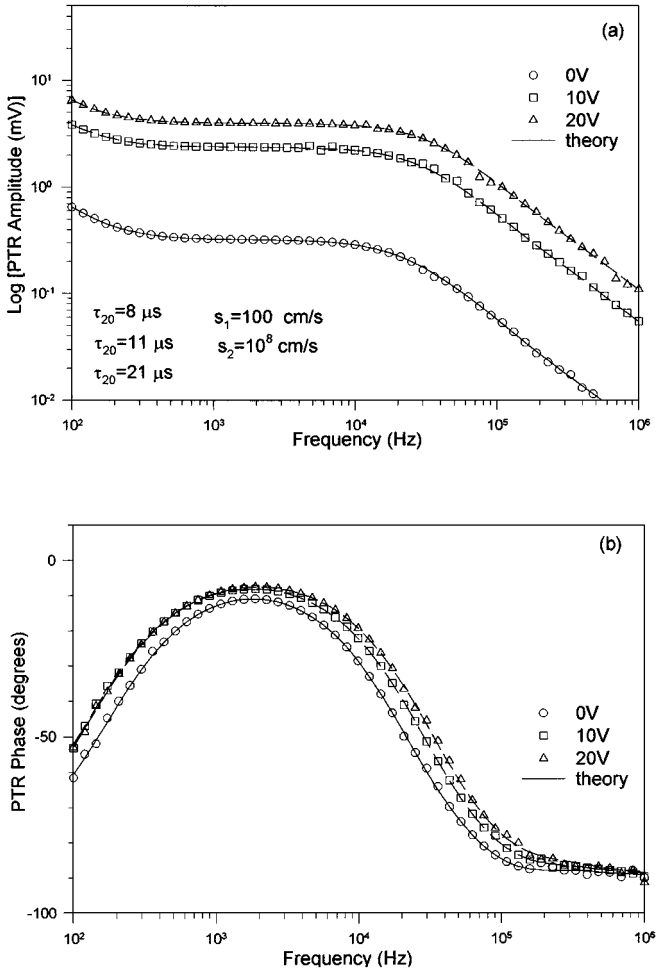

FIG. 6. Amplitude (a) and phase (b) of the PTR signal frequency scan of the device of Figs. 1(b) and 4. D, τ, s_1, and s_2 values as in Fig. 4. Best-fitted β value: 1.0 cm^2/s. Best fitted b-value, Eq. (8a), for all three curves: 1×10^{-16} MKS units; best-fitted a-values: 3.8×10^6 MKS ($V=0$); 2×10^5 MKS ($V=10$ V); and 5.5×10^4 MKS ($V=20$ V).

Figure 6 shows the PTR frequency scans from the same sample. Both amplitude and phase have been fitted to the theory of Eq. (8a) with the subsidiary Eq. (13), for the thickness-integrated, free-carrier density, and Eq. (17) for the thickness-integrated thermal wave. In each of the various dc voltage-dependent curves the prefactors a and b in Eq. (8a) were adjusted accordingly, so as to produce additively the optimal overlap in thermal- and plasma-wave components. This was rather easy, as the thermal wave affects primarily the low-frequency end (<1 kHz), whereas the plasma wave dominates the high end. It is worthwhile to mention that the best fits used the lifetime-electronic diffusivity pairs measured from the PC data of Fig. 5, which indicates identical electronic PTR and PC signal production mechanisms. The low-frequency data were sensitive to the actual value of the thermal diffusivity of Si, which was found to be 1.0 cm^2/s, in excellent agreement with literature values.[24] The inserted value for the thermal conductivity of Si from the literature, $k=148$ W/m K,[25] was not a sensitive parameter of the fit.

Figure 7 shows the PTR equivalent of Fig. 5. The maximum applied bias (30 V) in both PC and PTR cases was

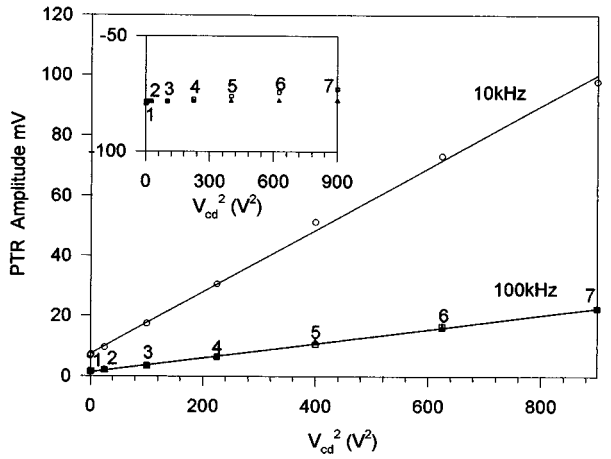

FIG. 7. Quadratic dependence of PTR signal amplitude and phase (inset) on applied dc bias of the bulk Si photoconductor for $f=10$ and 100 kHz. All parameters fitted into the 10 kHz curve are as in Fig. 5, including the theoretical best fit (τ, D) values to Eq. (8a). The value pair of the constants [a ($\times 10^5$ MKs), b [$\times 10^{-16}$ MKs]] are: (1: 38.0, 1.0); (2: 10.0, 1.0); (3: 2.0, 1.2); (4: 1.0, 2.0); (5: 0.55, 4.0); (6: 0.40, 7.0); and (7: 0.35, 10.0).

limited by the over-heating of the sample contacts due to the flow of high current densities. The minimum value is for $V=0$ V, as there is no need for an applied bias in order to obtain PTR signals. The agreement between the two sets of fitted values is excellent, as the same values of $\tau(V)$ and $D(V)$ were used for both figures. The quadratic dependence on V (and therefore on E) of the PTR amplitude should be noted in agreement with the theory [Eqs. (17)–(20)].

B. Thin-film polysilicon photoconductors

The PTR response of the device in the geometry of Fig. 1(a) is shown in Fig. 8. In this case, substantial increases of the applied bias resulted in only small changes in the PTR signals. This is due to the much higher resistivity exhibited by these thin films compared to the crystalline Si photoconductors. For all thin-film devices with lower doping density than 1×10^{15} cm^{-2}, there was no discernible difference in the PTR amplitude and phase responses between 0 and 60 V bias. Theoretical fits of Eq. (27) and of the modification of Eq. (17) as discussed in Sec. III D were produced and are also shown in Fig. 8. There was no possible operation based on the thin-film material values of E_x, μ_n, or τ_f, which would lead the theoretical curves to agree with the observed trends and shifts in both amplitude *and* phase of Fig. 8. The only way that a reasonable fit would be affected was by adjusting the values of the prefactor pair (a,b) in Eq. (8a), which tended to broaden the phase half-width by shifting the high-frequency wing while incurring no shift of the low-frequency wing. At the same time, knowledge of the substrate lifetime τ was an important input, as this is a parameter to which the curve-fitting is sensitive: This allowed the unique fixing of the surface thin-film photoconductor layer lifetime τ_f, a very important parameter for the operation of the photoconductive device and quite difficult to obtain otherwise.

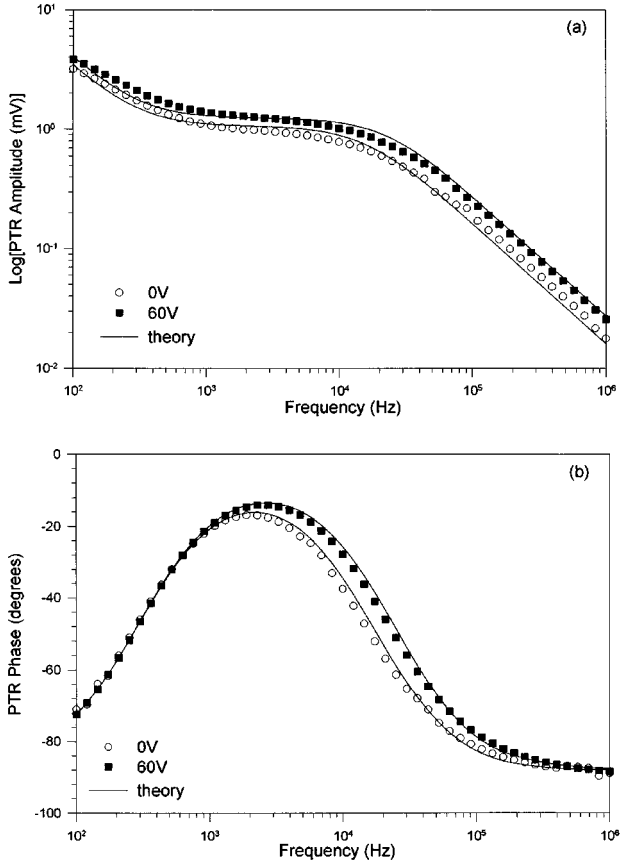

FIG. 8. Amplitude (a) and phase (b) of the PTR signal frequency scan of the thin-film device of Fig. 1(a). All substrate parameters were assigned the values found for the bulk crystalline Si photoconductor at zero bias. Thin-film values: $D_f=9$ cm^2/s; $d=1$ μm; $\beta_f=0.1$ cm^2/s; $k_f=15$ W/m K; $s=10^4$ m/s; $\tau_f=11$ μs ($V=0$ V), and 6 μs ($V=60$ V).

The change of the value pair (a,b) is expected with increased $V_{\rm dc}$, owing to the rise of the background dc temperature of the sample. The set of parameter values shown in the caption of Fig. 8 includes several to which the fit is relatively insensitive, such as the thermophysical properties of the thin film. This fact is expected, because the thin film is entirely thermally thin and the PTR technique cannot measure thermal transport across its bulk. In any case, it should be remembered that the presence of the thin film in the theory appears only in the front-surface boundary condition [Eq. (29)]. Similarly, its weight on the value of the PTR phase is insignificant at low frequencies, where the thermal-wave power centroid lies well within the substrate, as shown in Fig. 8(b). Nevertheless, the technique is sensitive enough to the thin-film lifetime at high frequencies; this parameter determines the position of the maximum of the phase curve. The sensitivity of the theoretical fit to the remaining parameters of Fig. 8 is low. Unfortunately, a theoretical fit to the PTR signal vs $V_{\rm dc}$ for the thin-film photoconductors does not yield meaningful results either, because the simultaneous adjustment of τ_f, a, and b is needed, leading to nonunique parameter sets, unless detailed fittings are performed at each and every level of applied bias.

Finally, the PC frequency spectra of the thin-film photoconductors were also obtained and are shown in Fig. 9. The

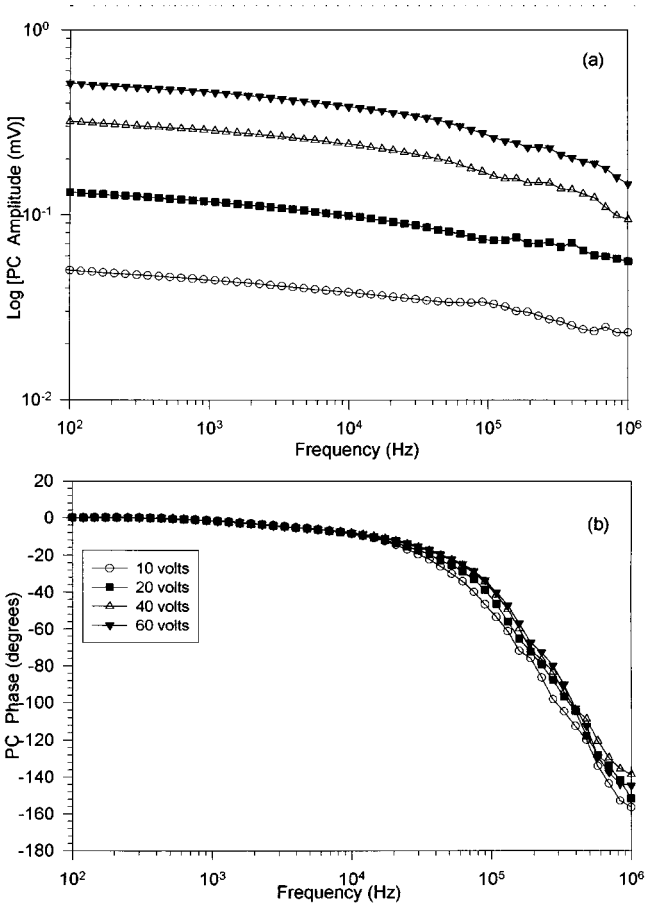

FIG. 9. Amplitude (a) and phase (b) of the photocurrent spectrum of the thin-film photoconductor of Fig. 1(a), whose PTR response is shown in Fig. 8.

remarkable features of these curves are (i) the gentle downward slope of the amplitude starting at very low frequencies, and (ii) the very strong phase lag exhibited above $\approx$50 kHz. The drift-current-density approach of the bulk crystalline Si photoconductors was unsuccessful in modeling these features. There is little doubt that the small increasing shifts of the PC phase-drops to higher frequencies with increasing bias are associated with the decrease in the thin-film electronic lifetime as a result of temperature rise. Incorporation of a lateral diffusion-current component to J_n in Eq. (30), with or without the presence of internal electric-field gradients along (x), was also unsuccessful. The transit-time concept of the photogenerated carriers to the electrodes via a lattice-scattering mechanism was considered, but was also unable to account for the behavior of Fig. 9: Satellite experiments indicated that the boundary of the illuminated region away from the cathode shifts the PC amplitude curve rigidly downward with increasing distance, without changes in the shape of the frequency response; it also leaves the phase unchanged. It is believed that the interpretation of these results resides with the fractal nature of plasma diffusion in the across-the-grain-boundary microregions of the LPCVD polysilicon thin films,[26,27] and this hypothesis is currently under investigation.

V. CONCLUSIONS

Infrared photothermal radiometry and photocurrent detection were utilized both theoretically and experimentally to analyze the performance of bulk crystalline Si and LPCVD polysilicon thin-film photoconductive devices. The developed theory was fitted to the data from the former samples. It yielded excellent agreements leading to information on the dependence of the recombination lifetime on the background temperature of the device, via heat release due to the Joule effect: Detectivity increased at the expense of frequency-response bandwidth.

The theoretical development was also applied to the data from the most highly implanted polysilicon device and yielded quantitative values for the mean recombination lifetime of the thin film, as distinct from that of the substrate Si. Much more modest increase in the detectivity with bias was observed in these structures, however, accompanied by a smaller decrease in detection bandwidth, owing to the much higher resistivity of these granular photoconductors.

The PTR technique has the advantage of treating the thin film as a lumped thermoelectronic element by probing its totally thermally thin dimension without regard to its lateral microstructure. As a consequence, one can obtain quantitative information about the mean lifetime of this device in a relatively straightforward manner, even though the details of the microstructure are not yet fully elucidated. On the contrary, the PC signal is dominated by transport across the domains of the microstructure, which makes the determination of the lifetime difficult or impossible without sophisticated analytical considerations.

[1] A. Mandelis and E. K. M. Siu, Phys. Rev. B **34**, 7209 (1986).
[2] E. K. M. Siu and A. Mandelis, Phys. Rev. B **34**, 7222 (1986).
[3] I. N. Bandeira, H. Closs, and C. C. Ghizoni, J. Photoacoust. **1**, 275 (1982).
[4] S. J. Sheard, M. G. Somekh, and T. Hiller, Mater. Sci. Eng. B **5**, 101 (1990).
[5] A. Salnick, A. Mandelis, and C. Jean, Solid-State Electron. (in press).
[6] W. Monch, *Semiconductor Surfaces and Interfaces* (Springer, Berlin, 1995).
[7] R. A. Budiman, A. Mandelis, H. E. Ruda, I. P. Koutzarov, and Q. Liu (unpublished).
[8] *Photoacoustic and Thermal-Wave Phenomena in Semiconductors*, edited by A. Mandelis (North-Holland, New York, 1987).
[9] S. Sheard and M. Somekh, in *Progress in Photothermal and Photoacoustic Science and Technology*, Vol. II: *Nondestructive Evaluation (NDE)*, edited by A. Mandelis (Prentice Hall, Englewood Cliffs, NJ, 1994), pp. 112–150.
[10] A. Othonos, C. Christofides, and A. Mandelis, Appl. Phys. Lett. **69** 821 (1996).
[11] S. J. Sheard and M. G. Somekh, Infrared Phys. **28**, 287 (1988).
[12] H. P. Baltes, in *Progress in Optics*, edited by E. Wolf (North-Holland, Amsterdam, 1976), Chap. I.
[13] E. A. Ulmer and D. R. Frankl, in *Proceedings of the Ninth International Conference on Physics Semiconductors* (Nauka, 1968), pp. 170–174.
[14] A. Mandelis, A. Budiman, and M. Vargas, in *Semiconductors and Semimetals: Effects of Disorder and Defects in Ion-Implanted Semiconductors; Optical and Photothermal Characterization*, edited by C. Christofides and G. Ghibaudo (in press).
[15] S. Ramo, J. R. Whinnery, and T. Van Duzer, *Fields and Waves in Communication Electronics* (Wiley, New York, 1965), p. 334.
[16] A. Mandelis, in *Photoacoustic and Thermal-Wave Phenomena in Semiconductors*, edited by A. Mandelis (North-Holland, New York, 1987), Chap. 15.
[17] J. Vanniasinkam, A. Mandelis, S. Buddhudu, and M. Kokta, J. Appl. Phys. **75**, 8090 (1994).

[18] J. P. McKelvey, *Solid State and Semiconductor Physics* (Harper and Row, New York, 1966), Chap. 10.
[19] D. T. Stevenson and R. J. Keyes, J. Appl. Phys. **26**, 190 (1955).
[20] A. Mandelis, J. Appl. Phys. **78**, 647 (1995).
[21] W. Shockley and W. T. Read, Phys. Rev. **87**, 835 (1952).
[22] G. E. Jellison and H. H. Burke, J. Appl. Phys. **60**, 841 (1986).
[23] R. F. Pierret, in *Advanced Semiconductor Fundamentals*, edited by R. F. Pierret and G. W. Neudeck (Addison-Wesley, Reading, MA, 1987), Vol. VI, Chap. 5.
[24] Y. S. Touloukian, R. W. Powell, C. Y. Ho, and M. C. Nicolaou, *Thermophysical Properties of Matter* (IFI/Plenum, New York, 1973), Vol. X.
[25] M. Neuberger, *Group IV Semiconducting Materials* (Plenum, New York, 1971).
[26] A. C. Boccara and D. Fournier, in *Photoacoustic and Thermal-Wave Phenomena in Semiconductors*, edited by A. Mandelis (North-Holland, New York, 1987), p. 308.
[27] L. J. Inglehart, A. Broniatowski, D. Fournier, A. C. Boccara, and F. Lepoutre, Appl. Phys. Lett. **56**, 1749 (1990).